RSC Advances

PAPER

View Article Online
View Journal | View Issue

Cite this: *RSC Adv.*, 2016, **6**, 17354

Bipyridine type Co-complexes as hole-transporting material dopants in perovskite solar cells†

Jiajiu Ye,[ab] Li Zhou,[a] Liangzheng Zhu,[ab] Xuhui Zhang,[ab] Zhipeng Shao,[a] Xu Pan*[a] and Songyan Dai*[c]

Received 3rd December 2015
Accepted 27th January 2016

DOI: 10.1039/c5ra25753k

www.rsc.org/advances

Hole-transporting materials (HTM) have significant effects on solar cell properties and cobalt complexes are commonly used as dopants in the HTM layer. The molecular structure of the ligands always has an important influence on the capability of the dopant. In this work, a series of substituted bipyridine cobalt complexes were synthesized by modification of the molecular structure and were investigated as possible dopant alternatives. Their electron conductive ability and redox potentials were tested by characterizing their absorption spectroscopy and conductivity properties. The best dopant, based on tris(4,4′-di-*tert*-butyl-2,2′-dipyridyl)-cobalt(III) tris[bis(trifluoromethylsulfonyl)-imide], resulted in a power conversion efficiency of up to 14.91% measured under standard solar conditions (AM 1.5G, 100 mW cm^{-2}). In addition, the co-solvent system of dichloroethane and acetylacetone was specifically selected for the bipyridine type dopants due to the greater solubility of both spiro and the dopant in this system. Because of the easy acquisition of the ligand and the simplicity of the synthesis of the complexes, this dopant represents a practical alternative as an efficient dopant for hole-transporting materials in perovskite solar cells.

Introduction

In recent years, organic–inorganic hybrid solar cells, as a new branch of solar cells, have undergone rapid development.[1–5] In 2009, the Miyasaka research team successfully prepared the first perovskite solar cell using an organic–inorganic hybrid material, and achieved a power conversion efficiency of 3.8%. In 2012, Park *et al.* reported spiro-OMeTAD as a HTM used in solid state organic/inorganic perovskite solar cells (PSC) to replace liquid ones, and got a photoelectric conversion efficiency of 9.7%.[6] Up to now, the efficiency of PSCs have exceeded 20%.[7–9]

In a perovskite solar cell, the HTM layer is important in determining the overall performance[10,11] and tremendous improvements of HTMs have been made in order to achieve high efficiency solar cells.[12–14] Among all the HTMs, spiro-OMeTAD (2′,7,7′-tetrakis-(*N*,*N*-di-*p*-methoxyphenylamine)-9,9′-spirobifluorene) is widely used in perovskite-based photovoltaic devices. The pristine form of spiro-OMeTAD possesses low conductivity, which would lead to low charge mobility and high series resistance. In order to solve this problem, an effective method of doping was used. Studies have shown that the key factors affecting efficient doping were the conductivity of the pure materials and their redox state. Utilizing spiro-OMeTAD$^+$ in an oxidized state can enhance the conductivity, which will directly affect the performance of the device.[15–18] So far, a series of effective cobalt dopants has been developed, and all of these dopants have allowed devices to exhibit excellent performance. Co(III) complexes of tris[2-(1*H*-pyrazol-1-yl)-4-(*tert*-butylpyridine) cobalt(III)tris(bis(trifluoromethylsulfonyl)imide)] (FK209) were used earlier in solid-state dye-sensitized solar cells by Burschka.[19] In 2013, Noh made use of FK209 as dopants in a spiro system and achieved a PCE of 10.4%, due to the effect between the Co-complex and Li-TFSI in conjunction with spiro-OMeTAD.[20] Koh developed a pyrimidine core cobalt dopant with a deep redox potential named MY11, and an overall power conversion efficiency of 12% was achieved using that as a p-type dopant of spiro-OMeTAD.[21] In addition, the role of the solvent is also important. Xu reported a low-cost, chlorinated organic solvent, where 1,1,2,2-tetrachloroethane (TeCA) was used as a co-solvent and an effective additive for a triarylamine-based organic HTM, significantly increasing the electrical conductivity. A record power conversion efficiency (PCE) of 7.7% was obtained.[22]

Despite the obvious effect of dopants, there are still defects. Some of the cobalt reacts with the organic host and the color of the HTM solution becomes dark, absorbing light and resulting in competition with the photosensitizer. Some of these dopants have poor solubility in organic solvents or possess a high boiling point, making photovoltaic device fabrication difficult.

[a]*Key Laboratory of Novel Thin-Film Solar Cells, Institute of Applied Technology, Hefei Institutes of Physical Science, Chinese Academy of Sciences, Hefei 230031, China*
[b]*University of Science and Technology of China, Hefei 230026, China*
[c]*State Key Laboratory of Alternate Electrical Power System with Renewable Energy Sources, North China Electric Power University, Beijing 102206, China*

† Electronic supplementary information (ESI) available. See DOI: 10.1039/c5ra25753k

Due to the complex synthetic method and high cost, most dopants are not easy to obtain which would limit large-scale production. Therefore, studies to find low-cost, colorless, easy to acquire dopants with good solubility for HTMs are still necessary.

In this work we report a number of substituted bipyridine cobalt complexes that have been synthesized from solution and are particularly promising due to their chemical properties of ambient stability, easy preparation, and the possibility to change the organic host chemical and physical properties. These cobalt complexes were employed as possible alternative dopants of spiro-OMeTAD in perovskite solar cells. In addition, we employed a dichloroethane and acetylacetone co-solvent as the HTM solvent. This was more efficient in doping triarylamine-based hole-conductors due to the improvement in solubility and the synergistic reaction between the co-solvent and dopant. An efficiency of 14.91% was obtained with a J_{sc} of 19.52 mA cm^{-2}, V_{oc} of 1.02 V, and FF of 74.96% based on tris(4,4′-di-*tert*-butyl-2,2′-dipyridyl)-cobalt(III)tris[bis(trifluoromethylsulfonyl)-imide] (D1). This work provides new alternatives for the fabrication of low-cost and efficient perovskite solar cells.

Experimental

Synthesis of cobalt complexes

All of the complexes depicted in Fig. 1 were synthesized and purified using similar procedures. In short, 3 molar equivalents of the ligand were dissolved in a methanol and water solvent mixture under magnetic stirring, and the solution was heated to 60 °C. The amount of methanol and water was adjusted according to the ligand solubility and the scale of the reaction so that the ligand was totally dissolved. Then, 1 molar equivalent of cobalt(II)perchlorate hexahydrate was added, and the mixture was stirred for 30–60 minutes. After the mixture cooled to room temperature, H_2O_2 and HCl were added at 5 minute intervals sequentially in order to oxidize the divalent cobalt and the mixture was heated at 75 °C for 2 hours. A concentrated lithium bis(tri-fluoromethanesulfonyl)imide/water solution was added slowly at first at room temperature to precipitate the crude product, which was then filtered and dried at 60 °C. The resulting compound was re-dissolved in methanol at 60 °C and then cooled down to 5 °C, and the crystallized solid was just the purified product (a solid that varied from light brown to yellow).

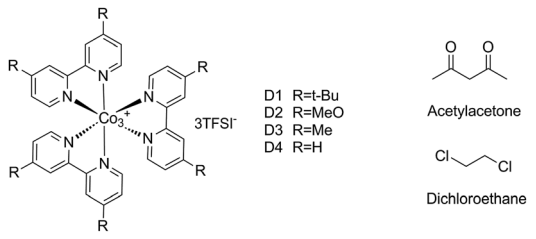

Fig. 1 Structure of cobalt complexes with different organic groups and composition of the co-solvent.

The product was characterized by ^{1}H-NMR and elemental analysis (details are described in ESI†).

Solar cell device fabrication

A thick dense blocking layer of TiO_2 (bl-TiO_2) was deposited onto a F-doped SnO_2 (FTO) substrate by spin coating to prevent direct contact between the FTO and the hole-conducting layer. This was carried out using a blocking layer precursor solution prepared from titanium(IV)isopropoxide $Ti[OCH(CH_3)_2]_4$ mixed with 2-methoxyethanol ($CH_3OCH_2CH_2OH$) and ethanolamine ($H_2NCH_2CH_2OH$) according to a reported method.[23] The film was then calcined at 500 °C. A mesoporous TiO_2 film layer (dysol, particle size: about 30 nm, crystalline phase: anatase) of about 200 nm thickness was deposited by spin coating at 3000 rpm for 30 s onto the bl-TiO_2/FTO substrate and calcined at 500 °C to remove organic components. The films were then immersed in a 50 mM $TiCl_4$ aqueous solution diluted with cool water at 65 °C for 0.5 h and were then heated to 500 °C to repair the surface of the mesoporous TiO_2 and improve the interfacial contact. Prepared MAI powders and PbI_2 (Aldrich) to form a 1.1 M $MAPbI_3$ solution were stirred in a mixture of DMSO and DMF (8.5 : 1.5 v/v) at 60 °C for 1 h. The resulting solution was coated onto the mp-TiO_2/bl-TiO_2/FTO substrate by a consecutive two-step spin-coating process at 1000 and 6000 rpm for 20 s and 30 s respectively. During the second spin-coating step, for the final 10 s, the substrate was treated with toluene drop-casting to form the perovskite crystal. CH_3NH_3I was synthesized from hydroiodic acid reacting with the methylamine, according to ref. 3. The HTM layer was deposited by spin-coating at 4000 rpm for 20 s, using a solution of spiro-MeOTAD, 4-*tert*-butylpyridine, and lithium bis(trifluoromethylsulphonyl)imide and the Co(III)-complex in dichloroethane/acetylacetone. Finally, a gold (80 nm) counter electrode was deposited by thermal evaporation on top of the device to form the back contact.

Characterization

The conductances of the spiro-OMeTAD complexes were measured by a Four-Point Probes tester (RTS-9). The thickness of the spiro-OMeTAD films deposited on a glass substrate was about 250 nm. The PCE and *J–V* curves were measured using

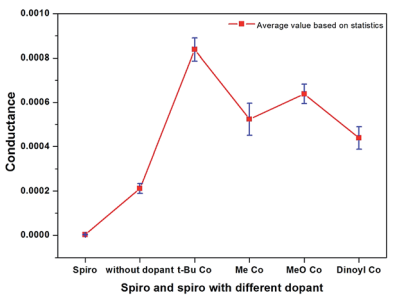

Fig. 2 Average conductance values of spiro-OMeTAD with dopant films on glass substrates. The thickness of the spiro-OMeTAD films deposited on a glass substrate is about 250 nm. The conductance values are normalized relative to the pristine spiro-OMeTAD film.

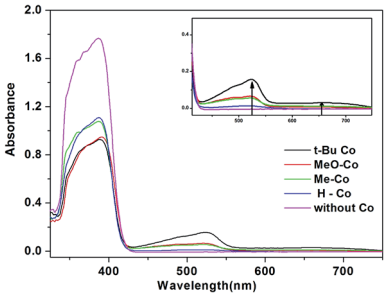

Fig. 3 UV absorption spectra of spiro-OMeTAD with additives (LiTFSI and TBP) and various Co dopants. The inset shows the enlarged spectra of the oxidized spiro-OMeTAD peak at around 523 nm. All solutions contained the same concentration of spiro-OMeTAD (2×10^{-5} M).

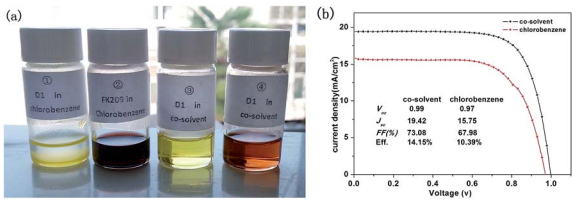

Fig. 4 (a) Co-complexes (D1) with *t*-Bu group in different solvents. ① and ③ in the picture are the Co-dopant in chlorobenzene and the co-solvent respectively, ② and ④ are spiro with TBP, Li-TFSI and Co-dopant in chlorobenzene and the co-solvent. (b) The *J*–*V* curves of the D1 dopant in different solvents.

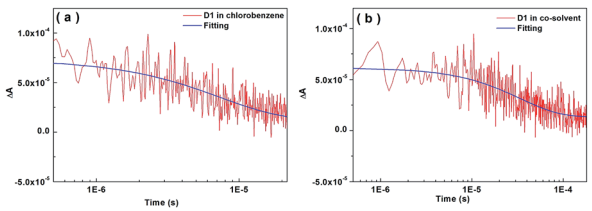

Fig. 5 TAs response of TiO_2/perovskite/HTM. (a) HTM layer with D1 dopant in chlorobenzene, measured with a pump light wavelength of 500 nm and a probe light wavelength of 1100 nm through detecting the spiro cation. The blue solid line represents the fitting result with one exponential function with a recombination time of 7.36 μs. (b) HTM layer with D1 dopant in co-solvent. The red curves are the results of the samples without and with D1 dopant, with a recombination time of 34.06 μs.

a solar simulator (Newport, Oriel Class A, 91195A) with a source meter (Keithley 2420) at 100 mA cm^{-2} AM 1.5G illumination and a calibrated Si-reference cell certified by NREL. The *J*–*V* curves for all devices were measured by masking the active area with a black mask of area 0.09 cm^2. UV-vis absorption spectra were recorded on a UV-vis spectrometer (Hitachi U-3300). Spiro-MeOTAD and additives were dissolved in the co-solvent. Incident photon to current efficiency (IPCE) measurements were confirmed as a function of wavelength from 300 to 800 nm (PV Measurements, Inc.), with a dual xenon/quartz halogen light source measured in DC mode with no bias light used. The setup

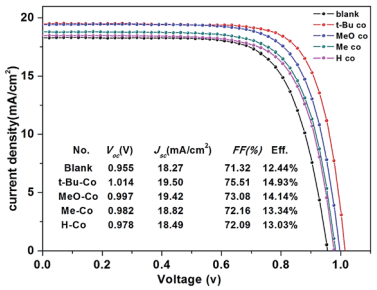

Fig. 6 Photocurrent–voltage (*J*–*V*) characteristics (light intensity: 100 mW cm^{-2}, AM 1.5G) of various dopants. A concentration of 6% dopant was added in mol% relative to spiro-MeOTAD. The preparation of HTM formulation was achieved by mixing a solution of 75 mg spiro-MeO-TAD, 18 μL LiTFSI, 29 μL TBP in 0.7 ml dichloroethane and different concentrations of Co-dopants (300 mg ml^{-1} in MeCN) in 0.3 ml acetylacetone (dichloroethane : acetylacetone = 7 : 3, v/v).

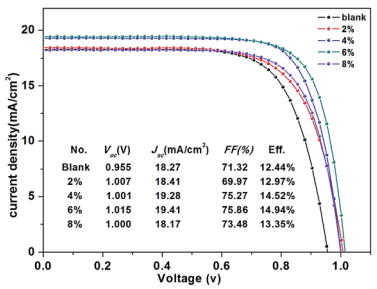

Fig. 7 Photocurrent–voltage (*J*–*V* curves) of devices based on different concentrations of doping. The percentages given in the legend are the amount of Co(III) added to the solution in mol% relative to spiro-MeOTAD.

was calibrated with a certified silicon solar cell (Fraunhofer ISE) prior to measurements. Transient absorption spectra (TA) were recorded on an LK80 (Applied Photophysics). The cells were measured before evaporating a gold counter with a pump light wavelength of 500 nm, a probe light wavelength of 1100 nm, and a repetition rate of 5 Hz. The energy of laser device was 150 μJ cm^{-2}.

Results and discussion

In mesoscopic $MAPbI_3$ perovskite solar cells, the pores of the mesoscopic TiO_2 layer are infiltrated by the $MAPbI_3$ perovskite crystal. On top of the mesoscopic TiO_2, there is a thin overlayer of perovskite where the HTM is covered. The electron–hole pairs are generated by the $MAPbI_3$ photosensitizer, and the generated electrons and holes are transported into the mesoscopic TiO_2 and HTM layer respectively upon the illumination of light. Therefore, the device will perform better if the HTM can extract the holes from the $MAPbI_3$ perovskite layer more effectively. Earlier research has already reported that cobalt compounds such as FK102, FK269, FK209, MY11 *etc.* can be used as efficient p-dopants for the HTM. The introduction of these dopants in the HTM layer is well-known to increase the conductivity in order to reduce the series resistance as well as the charge-

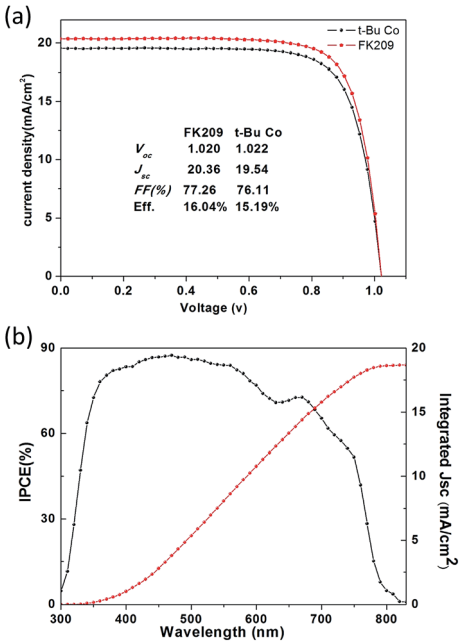

Fig. 8 *J*–*V* and IPCE characteristics for the best cell obtained in this study. (a) *J*–*V* curves of forward and reverse bias sweeps for the solar cell, and (b) corresponding incident photon-to-current conversion efficiency (IPCE) and integrated J_{sc} spectra.

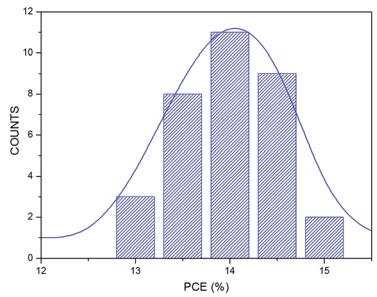

Fig. 9 Histogram of device PCE based on the spiro HTM system by doping cobalt complexes in co-solvent (measured from 33 devices).

transfer resistance at the interface between the HTM layer and the perovskite layer. The dopant can also assist the transformation of the reduced state of spiro-MeOTAD to the oxidized state. By incorporating different substituents, various cobalt complexes have been synthesized and used as dopants, and are shown in Fig. 1.

It is known that the hole conductivity of the HTM layer will affect the overall device performance and we believe that the additives will increase the conductivity and lead to an enhancement of the overall device performance. In order to understand the effect of doping, we measured the conductivity of spiro-OMeTAD films by using four-probe electrical conductivity measurements following a published procedure.[15,17,18,21]

The results are shown in Fig. 2. The average conductance values of spiro-OMeTAD films were tested based on parallel experiments. The conductivity of the pristine spiro film without dopant was 2.94×10^{-6} S cm^{-1}, which is similar to reported values.[21] The conductivity showed a significant increase when TBP and TFSI-Li were added, with values nearly two orders of magnitude times higher than the pristine spiro film. The conductivity of spiro-OMeTAD was further enhanced by doping with cobalt additives. The highest conductivity was attained for the spiro film with *t*-Bu Co dopant, with an increase from 2.11×10^{-4} to 8.38×10^{-4} S cm^{-1}, nearly a 4-fold increase compared to the film without cobalt dopant. Accordingly, the *t*-Bu Co dopant has an obvious effect and performs better than dopants with MeO and Me substituted groups, attaining the best performance.

To investigate the oxidation of spiro-OMeTAD by Co dopants, UV optical absorption spectroscopy was used. According to previous reports, the oxidized state of spiro would result in an absorption peak around 523 nm, which will not interfered with by neutral spiro, spiro radical cation, or Co complexes. The UV-vis absorption spectra for spiro solutions in the co-solvent upon adding dopants D1, D2, D3, D4 and without dopant (the spiro solution in a co-solvent of dichloroethane and acetylacetone with the addition of TBP and TFSI-Li) are illustrated in Fig. 3. There is no absorption band of spiro-OMeTAD without dopant at 520 nm, but when various Co dopants were added, a new absorption band, with a peak maxima located at around 523 nm, was clearly observed. Additionally, we found a simultaneous increase in absorption that extended to 750 nm which was assigned to the absorption of the spiro-OMeTAD cation. This phenomenon may be attributed to the effect of both the cobalt dopant and the solvent. The trend of each dopant is shown in the inset of Fig. 3. Due to the driving force for the charge transport reaction of spiro-OMeTAD to its oxidized state, *t*-Bu Co has the strongest absorption peak, which contributes towards the high efficiency of the spiro-to-spiro$^+$ conversion. The second absorption peak belongs to MeO–Co, followed by the dopants of Me–Co and H–Co. This proved that the higher absorption peak at 523 nm that the dopant possesses, a greater spiro$^+$ amount is generated. This result coincided with an increase in the device performance.

The solvent also had a significant impact on the cells. In order to investigate the solvent effect, we screened some solvents to find an appropriate solvent for the bipyridine type Co-complexes. Herein, the solvent should dissolve the spin-coating formulation of HTM, which comprises the dopant, spiro-MeOTAD, lithium bis (trifluoromethylsulfonyl) imide (LiTFSI), and 4-*tert*-butylpyridine (TBP). It was found to be difficult for the formulation to be dissolved well in only one solvent and to make sure that the perovskite was not corroded by the solvent at the same time. Therefore we adopted a co-solvent system in which the HTM and each component have good solubility. The co-solvent consisting of dichloroethane and acetylacetone (v : v = 7 : 3) solvents (Fig. 1) demonstrated greater solubility of the Co complexes, and is quite different from chlorobenzene which is commonly used.

We compared D1 complexes dissolved in chlorobenzene and the co-solvent respectively, and as we can see from Fig. 4(a), D1 had a relatively poor solubility in chlorobenzene and the solution was cloudy due to the presence of insoluble precipitates (①

in the picture), but can be dissolved well in the co-solvent (③ in the picture). ② and ④ were HTM solutions with TBP, Li-TFSI and the Co-dopant in chlorobenzene and in the co-solvent respectively, and the corresponding colors were dark purple and orange red. The color of the pure spiro solution changed when dopants were added, and the D1 dopant was different from ordinarily used pyrazole-type additives which expressed a dark purple color. This will avoid competition with the photosensitizer for light absorption and thus increase device performance.

After was D1 dissolved in co-solvent, the conductivity of the HTM increased from 7.86×10^{-5} to 8.38×10^{-4} S cm^{-1}, which is nearly a 10.4-fold increase. Here we used transient absorption spectra (TAs) in order to detect the recombination time between the HTM layer and the TiO_2 layer. The results are shown in Fig. 5(a) and (b). The recombination time between the TiO_2 layer and the spiro layer of device using the co-solvent was 34.06 μs, which is longer than when using chlorobenzene which was 7.36 μs. The longer recombination time indicated a lower electron–hole recombination rate. The *J–V* curves are shown in Fig. 4(b), and these clearly confirm that the device with dopant using the co-solvent expressed better performance compared with when chlorobenzene was used.

In order to determine the influence of the dopants on the photovoltaic performance, we prepared PSCs employing the co-solvent in combination with spiro-MeOTAD as the hole conductor. The photovoltaic parameters of the PSCs are shown in Fig. 6.

The corresponding photovoltaic parameters are collected in the inset table of Fig. 6. The PCE trend of the devices based on the dopants demonstrates a slight increase. The device without Co-dopant showed a comparably low efficiency of 12.44% with a short-circuit photocurrent density (J_{sc}) of 18.27 mA cm^{-2}, an open-circuit photo voltage (V_{oc}) of 0.95 V, and a fill factor (FF) of 71.32%. The device employing D1 dopant (*t*-Bu–Co) as the dopant yielded an efficiency of 14.93%, which is considerably higher than the efficiencies of the devices obtained based on other Co-dopant dopants. This might be attributed to the increase in conductivity and charge-transport mobility in coordination with a small quantity of protons (H^+) that are generated by acetylacetone during the photoinduced photochemical reactions. We note that the lowest conversion efficiency of the device using the D4 dopant (H–Co) without a substituted group is 13.03%, which can be mainly ascribed to its relatively low FF. This might be a result of a lower conductivity and cobalt crystallizing between the interface when the film takes shape.

Dopant concentrations from 0 (blank)–8 mol% (the percentages are the amount of Co dopants added to the solution in mol% relative to spiro-MeOTAD) were investigated with Li-TFSI and TBP added. The corresponding *J–V* curves obtained are shown in Fig. 7, and the photovoltaic parameters are collected in the inset table. The devices were measured directly after device fabrication without any additional treatment. The device without dopant showed a relatively low efficiency of 12.44% after cell fabrication. A relatively low efficiency of the blank sample obtained can be ascribed to the low conductivity and high charge transport resistance of the non-doped hole transport layer. Through further optimization of the doping concentrations, the device fabricated with 6 mol% *t*-Bu Co dopant showed the best performance. The J_{sc} and V_{oc} values for this device increased from 18.27 mA cm^{-2} to 19.41 mA cm^{-2} and from 0.95 V to 1.01 V, yielding an overall PCE of 14.94%. This corresponds to an improvement of more than 20% compared to the efficiency of the device containing the non-doped HTM. This can be attributed to the enhanced solubility of the dopant in the co-solvent, which will lead to a better dispersion of the spiro-MeOTAD matrix, enhance charge transport and avoid the crystallization of the Co complexes during the spin coating process. However, the J_{sc} and V_{oc} values decreased at higher concentrations (8 mol%), and especially the FF, which might be attributed to the increased recombination due to recrystallized and unreacted dopant in the HTM component.

Fig. 8(a) and (b) shows *J–V* curves measured *via* reverse and forward bias sweeps for one of the best-performing solar cells and the incident photon-to-current conversion efficiency (IPCE) spectra using 6 mol% dopant, the average values of the device showed a J_{sc} of 19.52 mA cm^{-2}, a V_{oc} of 1.019 V, and a FF of 74.96% under AM 1.5G solar irradiance (100 mW cm^{-2}), yielding a PCE of 14.91%, which is close to the device based on FK209 dopant (ESI Fig. S2†). The calculated photocurrent from the IPCE spectrum is 19.37 mA cm^{-2} that agrees well with the measured J_{sc}. This study reveals that the Co-complexes can be used as an alternative method to increase the photon-to-electron conversion.

To check the reproducibility of the device performance by using cobalt dopant, we repeated the device fabrication using the optimal doping concentration of 6% mol, and the photovoltaic parameters are compared using histograms obtained from 33 integrated perovskite devices, shown in Fig. 9. As can be seen from the results, the devices performed well, the average PCE was 14.23%,and more than 80% of the devices showed PCEs above 13.5% under 1 sun conditions. The average J_{sc} and V_{oc} values were highly reproducible. The PCE data obtained from the cells shows a low standard deviation, indicating good reproducibility.

Conclusions

We synthesized a series of substituted bipyridine cobalt complexes as an HTM dopant and fabricated mesoscopic TiO_2/$CH_3NH_3PbI_3$ heterojunction solar cells using cobalt dopants in the co-solvent of dichloroethane and acetylacetone. The synthesized dopant shows excellent dopant properties in photovoltaic applications. Finally, we achieved a power conversion efficiency of 14.91% using the dopant under optimal conditions. The addition of the Co-complex to spiro-OMeTAD increased device performance, which was mainly due to the increase in the electron transport capability and the solubility of HTM by using co-solvent. Furthermore, the results of this study show that the method of doping not only improves the overall device performance, but also provides good reproducibility. It provides a new way for the fabrication of low-cost and efficient

perovskite solar cells. Further work on the study and the employment of this additive in different organic HTMs is in progress.

Acknowledgements

This work was financially supported by the National High Technology Research and Development Program of China under Grant no. 2015AA050602, the National Natural Science Foundation of China under Grant no. 21273242, and State Key Laboratory of Alternate Electrical Power System with Renewable Energy Sources (Grant No. LAPS14012).

Notes and references

1 J. Burschka, N. Pellet, S.-J. Moon, R. Humphry-Baker, P. Gao, M. K. Nazeeruddin and M. Grätzel, *Nature*, 2013, **499**, 316–319.
2 B. Conings, L. Baeten, T. Jacobs, R. Dera, J. D'Haen, J. Manca and H.-G. Boyen, *APL Mater.*, 2014, **2**, 081505.
3 N. J. Jeon, J. H. Noh, Y. C. Kim, W. S. Yang, S. Ryu and S. I. Seok, *Nat. Mater.*, 2014, **13**, 897–903.
4 H. Zhou, Q. Chen, G. Li, S. Luo, T.-b. Song, H.-S. Duan, Z. Hong, J. You, Y. Liu and Y. Yang, *Science*, 2014, **345**, 542–546.
5 D. Liu, J. Yang and T. L. Kelly, *J. Am. Chem. Soc.*, 2014, **136**, 17116–17122.
6 H.-S. Kim, C.-R. Lee, J.-H. Im, K.-B. Lee, T. Moehl, A. Marchioro, S.-J. Moon, R. Humphry-Baker, J.-H. Yum and J. E. Moser, *Sci. Rep.*, 2012, **2**, 591–598.
7 J.-H. Im, I.-H. Jang, N. Pellet, M. Grätzel and N.-G. Park, *Nat. Nanotechnol.*, 2014, **9**, 927–932.
8 N. J. Jeon, H. G. Lee, Y. C. Kim, J. Seo, J. H. Noh, J. Lee and S. I. Seok, *J. Am. Chem. Soc.*, 2014, **136**, 7837–7840.
9 A. Kojima, K. Teshima, Y. Shirai and T. Miyasaka, *J. Am. Chem. Soc.*, 2009, **131**, 6050–6051.
10 Y. Song, S. Lv, X. Liu, X. Li, S. Wang, H. Wei, D. Li, Y. Xiao and Q. Meng, *Chem. Commun.*, 2014, **50**, 15239–15242.
11 Z. Yu and L. Sun, *Adv. Energy Mater.*, 2015, **5**, 213–230.
12 U. Bach, D. Lupo, P. Comte, J. Moser, F. Weissörtel, J. Salbeck, H. Spreitzer and M. Grätzel, *Nature*, 1998, **395**, 583–585.
13 Y.-J. Kim, D.-T. Tung, H.-J. Choi, B.-J. Park, J.-H. Eom, K.-S. Kim, J.-R. Jeong and S.-G. Yoon, *RSC Adv.*, 2015, **5**, 52571–52577.
14 Z. Liang, S. Zhang, X. Xu, N. Wang, J. Wang, X. Wang, Z. Bi, G. Xu, N. Yuan and J. Ding, *RSC Adv.*, 2015, **5**, 60562–60569.
15 A. Abate, T. Leijtens, S. Pathak, J. Teuscher, R. Avolio, M. E. Errico, J. Kirkpatrik, J. M. Ball, P. Docampo and I. McPherson, *Phys. Chem. Chem. Phys.*, 2013, **15**, 2572–2579.
16 J. H. Heo and S. H. Im, *Phys. Status Solidi RRL*, 2014, **8**, 816–821.
17 D. Poplavskyy and J. Nelson, *J. Appl. Phys.*, 2003, **93**, 341–346.
18 H. J. Snaith and M. Gratzel, *Appl. Phys. Lett.*, 2006, **89**, 262114.
19 J. Burschka, F. Kessler, M. K. Nazeeruddin and M. Grätzel, *Chem. Mater.*, 2013, **25**, 2986–2990.
20 J. H. Noh, N. J. Jeon, Y. C. Choi, M. K. Nazeeruddin, M. Grätzel and S. I. Seok, *J. Mater. Chem. A*, 2013, **1**, 11842–11847.
21 T. M. Koh, S. Dharani, H. Li, R. R. Prabhakar, N. Mathews, A. C. Grimsdale and S. G. Mhaisalkar, *ChemSusChem*, 2014, **7**, 1909–1914.
22 B. Xu, E. Gabrielsson, M. Safdari, M. Cheng, Y. Hua, H. Tian, J. M. Gardner, L. Kloo and L. Sun, *Adv. Energy Mater.*, 2015, **5**, 2340–2346.
23 J. Y. Kim, S. H. Kim, H. H. Lee, K. Lee, W. Ma, X. Gong and A. J. Heeger, *Adv. Mater.*, 2006, **18**, 572–576.